INSTITUTE OF PHYSICS PUBLISHING SMART MATERIALS AND STRUCTURES
Smart Mater. Struct. **13** (2004) 1025–1035 PII: S0964-1726(04)82211-0

Adaptive multi-mode resonant piezoelectric shunt damping

Dominik Niederberger[1], Andrew Fleming[2], S O Reza Moheimani[2] and Manfred Morari[1]

[1] Automatic Control Laboratory, Swiss Federal Institute of Technology, ETHZ, CH-8092 Zurich, Switzerland
[2] Laboratory for Dynamics and Control of Smart Structures, School of Electrical Engineering and Computer Science, The University of Newcastle, Callaghan 2308, Australia

E-mail: niederberger@control.ee.ethz.ch

Received 5 December 2003, in final form 5 April 2004
Published 8 July 2004
Online at stacks.iop.org/SMS/13/1025
doi:10.1088/0964-1726/13/5/007

Abstract
Multiple-modes of structural vibration can be suppressed through the connection of an electrical impedance to the terminals of a bonded piezoelectric transducer. The so-called resonant shunts, one commonly used class of shunt impedances, provide good nominal damping performance but they are highly sensitive to variations in transducer capacitance and structural resonance frequencies. This paper introduces a new technique for the online adaptation of multi-mode resonant shunts. By minimizing the relative phase difference between a vibration reference signal and the shunt current, circuit component values can be optimally tuned online. Experiments on a cantilever beam validate the proposed technique and demonstrate the simplicity of implementation. The adaptive law converges quickly and maintains optimal performance in the presence of environmental uncertainties.

1. Introduction

Piezoelectric shunt damping is a popular technique for vibration suppression in smart structures. Techniques encompassed in this broad description are characterized by the connection of an electrical impedance to a structurally bonded piezoelectric transducer. Such methods do not require an external sensor, may guarantee stability of the shunted system [15], and do not require parametric models for design purposes.

Shunt circuits do not require a feedback sensor, and in some circumstances may not require any support electronics or power supply at all. Typically, a shunt damping strategy involves a specific impedance structure which is tuned experimentally to damp a number of targeted structural modes.

Piezoelectric shunt impedance designs have included resistors [9], inductive networks [23, 11], switched capacitors [3], switched networks [18, 4], negative capacitors [22], and active impedances [1]. Resonant shunt impedances [23] consisting of resistors, capacitors, and inductors are simple to design, and they offer considerable effective modal damping. The performance of resonant shunt circuits is known to be highly sensitive to variations in the transducer capacitance and structural resonance frequencies [10, 17]. This paper introduces a new technique for the online adaptation of multi-mode resonant piezoelectric shunt damping circuits.

When targeting low frequency structural modes or utilizing transducers of low capacitance, impractically large inductance values are typically required. Virtual inductors and Riodan gyrators [19] have been employed to implement large inductance values. Hollkamp [12] first demonstrated an adaptive single-mode shunt circuit by varying the value of a virtual inductor to minimize an RMS vibration signal. Virtual circuit implementations are complicated to construct, require a large number of high voltage components, and are generally unsuitable for damping more than two modes simultaneously.

The synthetic impedance [5] was introduced as a simplified technique for the implementation of piezoelectric shunt impedances. As shown in figure 2, the synthetic impedance consists of a voltage controlled current source and signal filter representing the desired admittance. As the

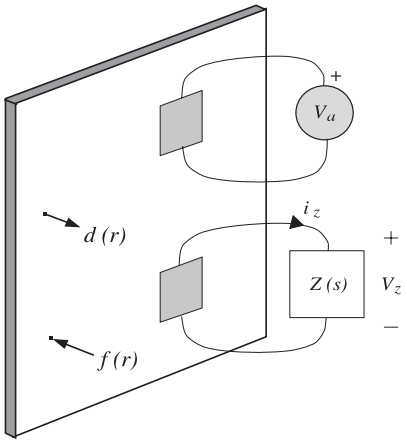

Figure 1. A general piezoelectric laminate structure excited by a point force $f(r, t)$, and the voltage V_a applied to a disturbance patch. The resulting vibration $d(r, t)$ is suppressed by the presence of an electrical impedance connected to the shunt transducer.

impedance seen by the transducer can be determined by a digital filter, the component values are easily tuned online. A technique exploiting this flexibility was presented in [6]. A multi-mode circuit was tuned online to minimize an RMS strain signal estimated from the terminal voltage. Although this method requires no vibration sensor, it is slow to converge and is dependent on the disturbance spectrum.

A new adaptive technique based on relative phase shift was presented in [17]. It was shown that minimizing the relative phase difference between a vibration reference signal and the shunt current results in optimal tuning of the circuit parameters. This technique is not based on a time averaged RMS estimate and is thus faster to converge and displays significantly less misadjustment at the minima. In [17] a single-mode shunt circuit was implemented through the use of a variable virtual inductance. In this paper, the results are extended to multiple modes with the utilization of a synthetic impedance. The impedance dynamics and adaptation rule are computed in real time on a digital signal processor.

This paper is organized into the following sections. In section 2, the modeling and dynamics of piezoelectric laminate structures is reviewed. In section 3, the adaptation rule and implementation details are presented. Experimental results in section 4 are followed by conclusions in section 5.

2. Modeling

Consider the piezoelectric laminate structure shown in figure 1. The goal is to suppress vibration resulting from two disturbances: V_a, the voltage applied to a disturbance patch, and $f(r, t)$, a point force located at the point r.

For generality, the objective is to model the effect of a shunted piezoelectric transducer on the known model of a mechanical structure. The open-loop, i.e. with no shunt attached, transfer functions required are

$$G_{va}(s) = \frac{V_p(s)}{V_a(s)} \qquad G_{vv}(s) = \frac{V_p(s)}{V_z(s)} \qquad G_{da}(r, s) = \frac{d(r, s)}{V_a(s)}, \tag{1}$$

where $V_p(s)$ is the piezoelectric voltage induced in the shunt transducer, and $d(r, s)$ is the displacement measured at a point r. If the disturbance and shunt transducer are identical, collocated, and poled in opposite directions as in figure 2, $G_{va}(s) = -G_{vv}(s)$.

The above transfer functions can be derived analytically, for example by solving the Euler–Bernoulli beam equation [8]. Alternatively, system identification [13] can be employed to estimate these models directly from experimental data.

Following the modal analysis procedure [14], the resulting transfer functions have the familiar form

$$G_{da}(r, s) = \frac{d(r, s)}{V_a(s)} = \sum_{k=1}^{\infty} \frac{F_k \phi_k(r)}{s^2 + 2\zeta_k \omega_k s + \omega_k^2}, \tag{2}$$

$$G_{vv}(s) = \frac{V_p(s)}{V_z(s)} = \sum_{k=1}^{\infty} \frac{\alpha_k}{s^2 + 2\zeta_k \omega_k s + \omega_k^2}, \tag{3}$$

where F_k, and α_k represent the lumped modal and piezoelectric constants applicable to the kth mode of vibration. Since G_{vv} is a collocated transfer function, $\alpha_k \geqslant 0$.

2.1. Modeling the presence of a shunt circuit

Using the open-loop transfer functions (1), the presence of an electrical impedance $Z(s)$ will now be incorporated into the structural dynamics. Referring to figure 2, the relationship between voltage and current in the Laplace domain is

$$V_z(s) = I_z(s) Z(s). \tag{4}$$

Applying Kirchhoff's voltage law we obtain

$$V_z(s) = V_p(s) - \frac{1}{C_p s} I_z(s), \tag{5}$$

where C_p represents the shunt transducer capacitance. Combining (4) and (5) we obtain

$$V_z(s) = \frac{Z(s)}{\frac{1}{C_p s} + Z(s)} V_p(s) \tag{6}$$

or

$$V_z(s) = \frac{C_p s Z(s)}{1 + C_p s Z(s)} V_p(s). \tag{7}$$

By applying the principle of superposition, the disturbance and shunt voltage strain contributions are

$$V_p(s) = G_{va}(s)\ V_a(s) + G_{vv}(s) V_z(s). \tag{8}$$

The shunted composite system can be obtained from equations (4), (5), and (8):

$$\frac{V_p(s)}{V_a(s)} = \frac{G_{va}(s)}{1 + G_{vv}(s) K(s)}, \tag{9}$$

where

$$K(s) = \frac{-Z(s)}{Z(s) + \frac{1}{C_p s}}. \tag{10}$$

The composite displacement transfer function can also be derived in a similar fashion:

$$\frac{d(r, s)}{V_a(s)} = \frac{G_{da}(r, s)}{1 + G_{vv}(s) K(s)}. \tag{11}$$

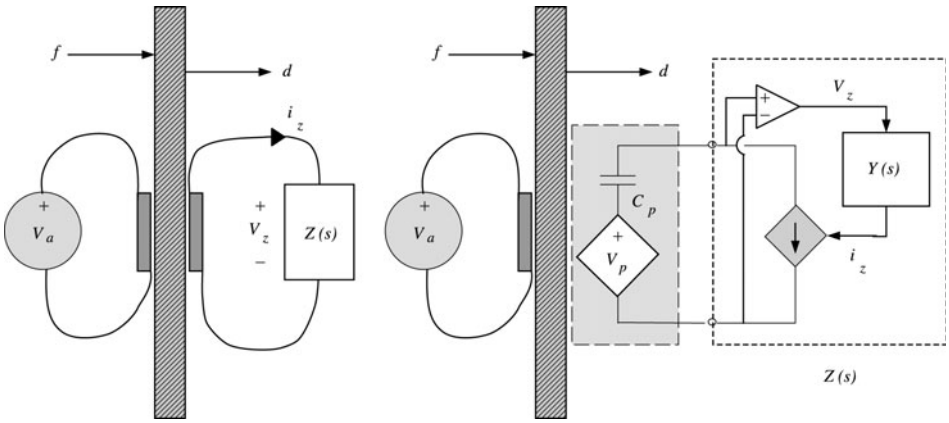

Figure 2. The physical and electrically equivalent view of a structure disturbed by an applied actuator voltage $V_a(s)$ and external force $F(r, s)$. The resulting vibration $d(r, s)$ is suppressed by the presence of a shunt impedance.

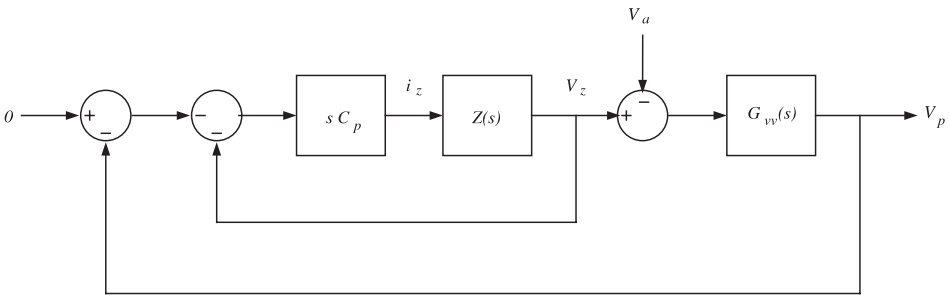

Figure 3. The strain-feedback interpretation of piezoelectric shunt damping with $G_{vv}(s) = -G_{va}(s)$.

By again applying the principle of superposition, the effect of force disturbance $F(r, s)$ located at point r can be included:

$$V_p(s) = \frac{1}{1 + G_{vv}(s)K(s)} \times (G_{va}(s)V_a(s) + G_{vf}(r, s)F(r, s)), \quad (12)$$

$$d(r, s) = \frac{1}{1 + G_{vv}(s)K(s)} \times (G_{da}(r, s)V_a(s) + G_{df}(r, s)F(r, s)), \quad (13)$$

where $G_{df}(r, s)$ and $G_{vf}(r, s)$ are the respective transfer functions from an applied force $F(r, s)$ to the displacement $d(r, s)$ and shunt transducer piezoelectric voltage V_p, i.e.

$$G_{vf}(r, s) = \frac{V_p(s)}{F(r, s)} \qquad G_{df}(r, s) = \frac{d(r, s)}{F(r, s)}. \quad (14)$$

From equation (9) it can be concluded that the presence of an electrical shunt impedance parameterizes an equivalent collocated strain feedback controller. A diagrammatic representation of equation (9) is shown in figure 3. Further interpretation and analysis can be found in [15].

In section 4, where the experiments are presented, the transfer function $G_v(r, s)$ from an actuator disturbance voltage $V_a(s)$ to the velocity $v(r, s)$ is measured to validate the performance of the proposed shunt controllers. This transfer function is defined as

$$G_v(r, s) = \frac{v(r, s)}{V_a(s)} = sG_{da}(r, s). \quad (15)$$

3. Adaptation law

In this section, a new adaptation law for multi-mode resonant shunts is derived. First, the *relative phase adaptation* of single-mode R–L shunts is reviewed, then it is extended to multi-mode resonant shunts.

3.1. Adaptive single-mode R–L shunt

As shown in section 2, an electrical shunt impedance parameterizes an equivalent collocated strain feedback controller. If the impedance $Z(s)$ is chosen as a series inductor–resistor network (R–L shunt), a resonant shunt controller is obtained that significantly reduces the vibration associated with a single structural mode [9]. As described in [10, 17], the damping performance of resonant shunts is sensitive to environmental variation in the structural resonance frequencies and transducer capacitance. Online tuning of the inductance L is required to maintain optimal damping. To this end, adaptive techniques based on root mean square (RMS) minimization [12], and relative phase shift [17] have been proposed. These two approaches, applied to an electromagnetic system, are compared in [16]. In that instance, relative phase adaptation tunes more quickly with less misadjustment than the RMS methodology. In the following, a review and extension of the relative phase adaptation is presented.

Relative phase adaptation is based on adjusting the relative phase difference between the velocity and shunt current to $-\pi/2$. A simple multiplication and filter operation evaluates the relative phase difference. Consider figure 2, where $Z(s) =$

$R + sL$. Inserting $V_z(s) = I_z(s)(R + sL)$ into equation (6) leads to

$$I_z(s) = V_\mathrm{p}(s)\frac{sC_\mathrm{p}}{s^2LC_\mathrm{p} + sC_\mathrm{p}R + 1}. \tag{16}$$

As V_p is dynamically proportional to the strain $x(s)$ experienced by the piezoelectric transducer, i.e. $V_\mathrm{p}(s) = cx(s) = c\nu(s)/s$, where c is a constant and $\nu(s)$ is the velocity, the transfer function $G_{I\nu}(s)$ from the velocity $\nu(s)$ to the current $I_z(s)$ can be expressed as

$$G_{I\nu}(s) = \frac{I_z(s)}{\nu(s)} = \frac{cC_\mathrm{p}}{1 + sC_\mathrm{p}R + s^2LC_\mathrm{p}}. \tag{17}$$

The phase of $G_{I\nu}(\mathrm{j}\omega)$ is

$$\angle(G_{I\nu}(\mathrm{j}\omega)) = \phi_n = -\tan^{-1}\left(\frac{\omega C_\mathrm{p}R}{1 - LC_\mathrm{p}\omega^2}\right). \tag{18}$$

According to [9], optimal tuning of the R–L shunt is achieved when $\omega_n = 1/(LC_\mathrm{P})$, where ω_n is the structural resonance frequency of the nth mode. From equation (18), one can see that this tuning condition can be reformulated by the condition $\angle G_{I\nu}(\mathrm{j}\omega_n) = -\pi/2$. A function $f_p(L, \omega_n) = \mathrm{sgn}\left(\angle(G_{I\nu}(\mathrm{j}\omega_n)) + \frac{\pi}{2}\right)$ can be defined that reveals the required tuning direction of the inductance value. The discrete adaptation of L that tunes the nth mode is given by

$$\begin{aligned} L_{k+1} &= L_k + \alpha\left(f_p(L_k, \omega_n)\right) \\ &= L_k + \alpha\mathrm{sgn}\left(\angle(G_{I\nu}(\mathrm{j}\omega_n)) + \frac{\pi}{2}\right), \end{aligned}$$

where α is the tuning constant. A direct evaluation of the phase angle is not straightforward and complicates the adaptation scheme shown above. A practical alternative for evaluating the tuning direction is shown in the following. If we assume that the velocity $\nu(t)$ and current $I_z(t)$ are tonal, a reasonable assumption as the resonances are very lightly damped, the multiplication of $\nu(t) = \sin(\omega_n t)$ with $I_z(t)$ can be written as

$$\nu(t)I_z(t) = \sin(\omega_n t)A_n\sin(\omega_n t + \phi_n),$$

where ϕ_n is the phase shift equal to $\angle(G_{I\nu}(\mathrm{j}\omega_n))$ and $A_n = |G_{I\nu}(\mathrm{j}\omega_n)|$. After some manipulations, the following expression can be obtained:

$$\nu(t)I_z(t) = A_n\left(\tfrac{1}{2}\left(\cos(\phi_n) - \cos(2\omega_n t + \phi_n)\right)\right). \tag{19}$$

By low-pass filtering the above expression with a cut-off frequency below $2\omega_n$, the second term can be neglected and one gets

$$g_\mathrm{LP}(t) * \left[\nu(t)I_z(t)\right] = \frac{A_n}{2}\cos(\phi_n), \tag{20}$$

where $g_\mathrm{LP}(t)$ represents the impulse response of a low-pass filter, and $*$ denotes the time domain convolution operator. It can be seen that

$$\begin{aligned} &\mathrm{sgn}\left(g_\mathrm{LP}(t) * \left[\nu(t)I_z(t)\right]\right) = \mathrm{sgn}(\cos(\phi_n)) \\ &\quad = \mathrm{sgn}\left(\angle(G_{I\nu}(\mathrm{j}\omega_n)) + \frac{\pi}{2}\right), \end{aligned}$$

for $-\frac{3\pi}{2} < \phi_n < \frac{\pi}{2}$. This technique constitutes a new means for evaluating the tuning direction. The discrete adaptation law can be rewritten as

$$L_{k+1} = L_k + \alpha\mathrm{sgn}\left(g_\mathrm{LP}(t) * \left[\nu(t)I_z(t)\right]\right). \tag{21}$$

By removing the sgn operator, effectively allowing the tuning rate to vary, the following continuous tuning law can be obtained:

$$\frac{\mathrm{d}L(t)}{\mathrm{d}t} = \beta\left(g_\mathrm{LP}(t) * \left[\nu(t)I_z(t)\right]\right), \tag{22}$$

where β is the tuning rate. Equation (22) represents the proposed relative phase adaptation law for single-mode R–L shunts.

3.1.1. More detailed convergence analysis. In reality, where the signals are not purely tonal, the signals $\nu(t)$ and $I_Z(t)$ can be generally written as

$$\nu(t) = \int_0^\infty S_\nu(\omega_\nu)\sin(\omega_\nu t + \phi_\nu(\omega_\nu))\,\mathrm{d}\omega_\nu, \tag{23}$$

$$I_z(t) = \int_0^\infty S_I(\omega_I)\sin(\omega_I t + \phi_I(\omega_I))\,\mathrm{d}\omega_I, \tag{24}$$

where $S_\nu(\omega)$ and $S_I(\omega)$ are the spectral densities of $\nu(t)$ and $I_z(t)$ respectively, and $\phi_\nu(\omega)$ and $\phi_I(\omega)$ the corresponding phase shifts. Since the current $I_z(t)$ is band-pass filtered by the $RC_\mathrm{p}L$-network, it can be assumed that $S_I(\omega)$ consists only of the signal of one mode. From equation (18), if the resonances are very lightly damped, we know that $G_{I\nu}$ changes its phase at $\omega_m = 1/\sqrt{LC_\mathrm{p}}$ from 0 to $-\pi$. Therefore, one can write $\phi_I(\omega) = \phi_\nu(\omega)$ for $\omega < \omega_m$ and $\phi_I(\omega) = \phi_\nu(\omega) - \pi$ for $\omega > \omega_m$.

The proposed relative phase adaptation law low-pass filters the multiplication of $\nu(t)$ and $I_z(t)$ (equation (22)) and converges to a value such that $g_\mathrm{LP}(t) * \left[\nu(t)I_z(t)\right] = 0$. As multiplication in the time-domain corresponds to a convolution in the frequency domain, we first calculate all possible low-pass filtered multiplication pairs $\Pi(\omega_\nu, \omega_I)$ between the two frequencies ω_ν and ω_I, respectively. One gets

$$\begin{aligned} &\Pi(\omega_\nu, \omega_I) \\ &\quad = g_\mathrm{LP}(t) * \left[S_\nu(\omega_\nu)\sin(\omega_\nu t + \phi_\nu)S_I(\omega_I)\sin(\omega_I t + \phi_I)\right] \\ &\quad = \tfrac{1}{2}S_\nu(\omega_\nu)S_I(\omega_I)g_\mathrm{LP}(t) * [(\cos((\omega_\nu - \omega_I)t + \phi_\nu - \phi_I) \\ &\qquad - \cos((\omega_\nu + \omega_I)t + \phi_\nu + \phi_I))] \\ &\quad = \begin{cases} 0 & : \omega_\nu \neq \omega_I \\ \frac{1}{2}S_\nu(\omega_\nu)S_I(\omega_I) & : \omega_\nu = \omega_I < \omega_m \rightarrow \phi_I = \phi_\nu \\ 0 & : \omega_\nu = \omega_I = \omega_m \\ -\frac{1}{2}S_\nu(\omega_\nu)S_I(\omega_I) & : \omega_\nu = \omega_I > \omega_m \rightarrow \phi_I \\ & \qquad = \phi_\nu - \pi. \end{cases} \end{aligned}$$

Thus, all frequencies $\omega_\nu = \omega_I < \omega_m$ contribute positively, all frequencies $\omega_\nu = \omega_I > \omega_m$ negatively, and all other frequencies do not contribute. The inductor value L will converge to a value such that for $\omega_m = 1/\sqrt{LC_\mathrm{p}}$ the positive contribution is equal to the negative contribution, i.e. $A_1 = A_2$ in figure 4(a). In order to have $g_\mathrm{LP}(t) * \left[\nu(t)I_z(t)\right] = 0$, the following must occur:

$$\begin{aligned} &\arg_{\omega_m}\left(\int_0^{\omega_m}\int_0^{\omega_m} S_\nu(\omega_\nu)S_I(\omega_I)\,\mathrm{d}\omega_\nu\,\mathrm{d}\omega_I\right. \\ &\qquad \left. - \int_{\omega_m}^{\infty}\int_{\omega_m}^{\infty} S_\nu(\omega_\nu)S_I(\omega_I)\,\mathrm{d}\omega_\nu\mathrm{d}\omega_I\right) = 0. \end{aligned}$$

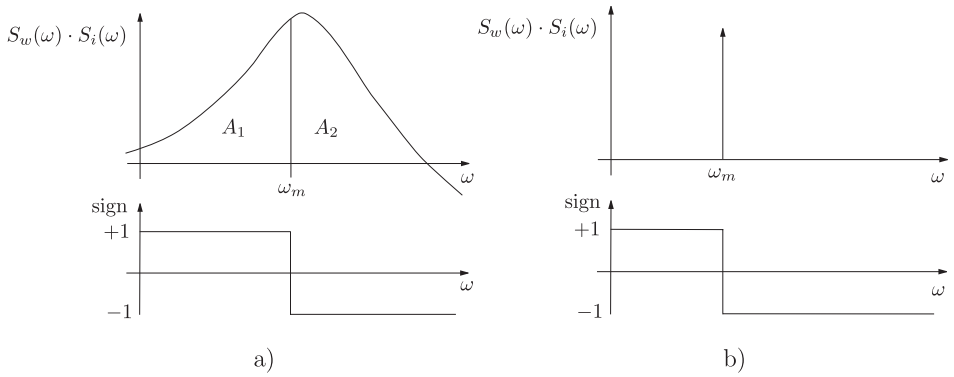

Figure 4. Convergence analysis, where the upper plots show the spectral density $S_v S_I$, and the lower, the sign of the tuning direction. In (a) the adaptation of L converges such that $1/\sqrt{LC_\mathrm{p}} = \omega_m$, where $A_1 = A_2$. In (b), the excitation is tonal and $1/\sqrt{LC_\mathrm{p}} = \omega_m$ converges to the excitation frequency.

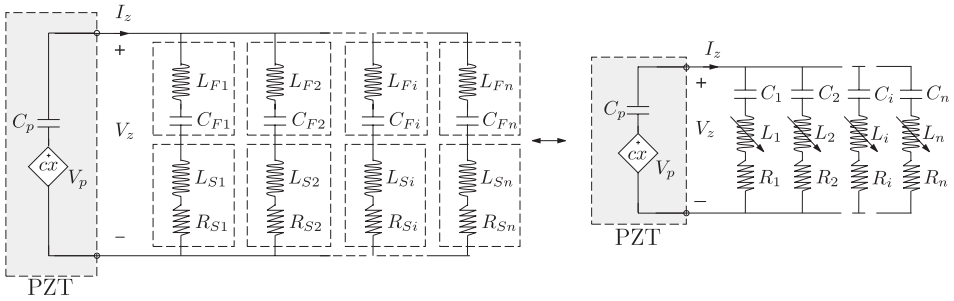

Figure 5. Current-flowing circuit and its simplification.

For example, if $S_v(\omega)S_I(\omega)$ is tonal with the frequency ω_m as shown in figure 4(b), the adaptation will converge to this frequency. Correspondingly, the adaptation does not necessarily act to minimize the $\mathcal{H}_2$ norm of the transfer function G_v. If the $\mathcal{H}_2$ norm of G_v is to be minimized, one can easily introduce compensators that add delay to the signals $v(t)$ and $I_z(t)$, such that the relative phase adaptation will converge to the frequency where the $\mathcal{H}_2$ is minimized. In [16], it was shown that the choice of these compensators can be made when the system is first commissioned. For example, an RMS methodology can be employed to set the compensators by minimizing the $\mathcal{H}_2$ norm [6]. If the spectral density of the disturbance is constant, after the compensators are set, the relative phase adaptation will always tune to minimize the $\mathcal{H}_2$.

3.2. Adaptive resonant multi-mode shunts

Multi-mode shunt damping techniques were introduced to allow the control of multiple structural modes with a single piezoelectric transducer. Wu [20, 21] proposed the so-called current-blocking techniques where a parallel capacitor and inductor are inserted in series with each single-mode shunt branch. One associated problem is the required circuit size to damp three or more modes: the order of the shunt circuit increases quadratically as the number of modes to be damped increases. Current-flowing circuits [2], such as that pictured in figure 5, are easier to tune and increase only linearly in order as a greater number of modes are to be shunt damped simultaneously. At a specific frequency ω_i, the inductor capacitor network $C_{Fi} - L_{Fi}$ allows current to flow through the rest of the branch; at all other frequencies the branch appears approximately as an open circuit. The damping inductor and resistor L_{Si}–R_{Si} acts analogously to a single-mode shunt circuit at the frequency ω_i. The circuit is simplified by combining the series inductors L_{Fi} and L_{Si} to L_i (figure 5 right).

In the following, the inductive elements in a current-flowing circuit will be adapted online to compensate for variation in structural resonance frequencies and transducer capacitance. In previous multi-mode techniques, the inductors have been tuned by minimizing a signal related to the RMS strain [6]. The branch inductor values were updated using a gradient search algorithm. As the performance function is rather flat around the optimum, this strategy is slow to converge and is prone to misadjustment after the minimum has been reached. A new technique based on relative phase adaptation will now be presented.

First, due to the series $C_{Fi} - L_{Fi}$ network, we notice that each branch can be regarded independently. The series $C_{Fi} - L_{Fi}$ network has zero impedance for $\omega = \frac{1}{\sqrt{C_{Fi}L_{Fi}}}$ and has high impedance at all other frequencies. Therefore, the transfer function from structural velocity to the current I_i in the ith branch can be written around the ith modal resonance frequency ($s \approx \mathrm{j}\omega_i$) as

$$G_i(s) = \frac{I_n(s)}{v(s)} = \frac{c}{s} \frac{s/L_i}{s^2 + s\frac{R_i}{L_i} + \frac{C_i + C_\mathrm{p}}{C_\mathrm{p} C_i L_i}}, \tag{25}$$

where the electrical resonance frequency is

$$\omega_{i_\mathrm{el}}^2 = \frac{C_i + C_\mathrm{P}}{C_i C_\mathrm{P} L_i} = \frac{1}{L_i C_{\mathrm{eq}_i}}. \tag{26}$$

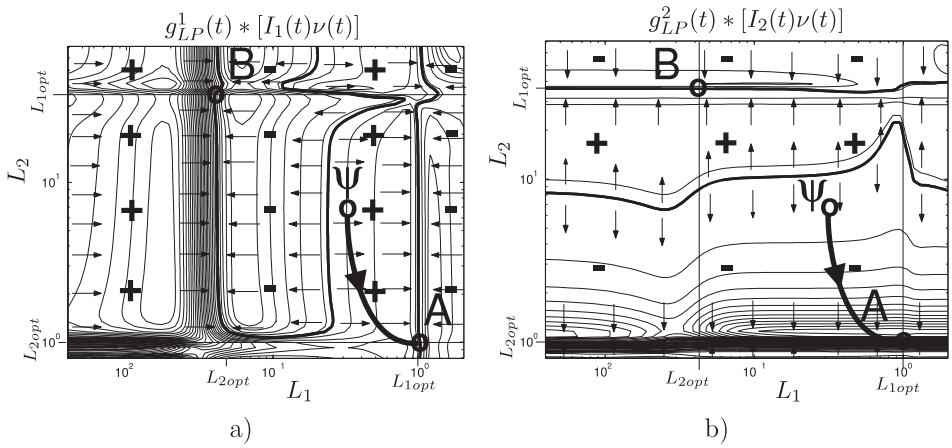

Figure 6. (a) $g^1_{\mathrm{LP}}(t) * [I_1(t)\nu(t)]$ and (b) $g^2_{\mathrm{LP}}(t) * [I_2(t)\nu(t)]$ as a function of the normalized L_1 and L_2.

The phase of $G_i(\mathrm{j}\omega)$ becomes

$$\angle(G_i(\mathrm{j}\omega)) = -\tan^{-1}\left(\frac{\omega R_i/(L_i)}{(C_i + C_\mathrm{p})/(C_i C_\mathrm{p} L_i) - \omega^2}\right), \quad (27)$$

and is $-\pi/2$ for $\omega_i = 1/\sqrt{C_{\mathrm{eq}_i} L_i}$ with $C_{\mathrm{eq}_i} = (C_i + C_\mathrm{p})/(C_i C_\mathrm{p})$. Thus we can use relative phase adaptation to tune the ith branch to the corresponding mechanical mode. As the branches naturally bandpass filter the current at the corresponding resonance frequency, no additional bandpass filters for the current signal are necessary. Velocity bandpass filters are not required either as long as the mechanical resonance frequencies are not harmonic. The adaptation of the inductor vector $\bar{L}(s)$ is

$$\frac{\partial \bar{L}(s)}{\partial t} = \begin{pmatrix} \dot{L}_1(t) \\ \dot{L}_2(t) \\ \vdots \\ \dot{L}_n(t) \end{pmatrix} = \begin{pmatrix} \alpha_1 g^1_{\mathrm{LP}}(t) * [\nu(t) I_1(t)] \\ \alpha_2 g^2_{\mathrm{LP}}(t) * [\nu(t) I_2(t)] \\ \vdots \\ \alpha_n g^n_{\mathrm{LP}}(t) * [\nu(t) I_n(t)] \end{pmatrix}, \quad (28)$$

where α_i is the ith tuning rate, and $g^i_{\mathrm{LP}}(t)$ is the ith low-pass filter with a cut-off frequency below $2\omega_i$.

3.3. Convergence analysis

In the following, a convergence analysis for a two mode shunt is presented. In this case, the tuning law is

$$\dot{L}_1(t) = \alpha_1 g^1_{\mathrm{LP}}(t) * [\nu(t) I_1(t)] \quad (29)$$

$$\dot{L}_2(t) = \alpha_2 g^2_{\mathrm{LP}}(t) * [\nu(t) I_2(t)]\,. \quad (30)$$

For a piezoelectric laminated beam structure, the tuning directions

$$dL_1 = \mathrm{sgn}\left(g^1_{\mathrm{LP}} * [\nu(t) I_1(t)]\right) \quad (31)$$

$$dL_2 = \mathrm{sgn}\left(g^2_{\mathrm{LP}} * [\nu(t) I_2(t)]\right) \quad (32)$$

for the update of L_1 and L_2 are plotted in figure 6. In figure 6(a), the tuning direction for L_1 is plotted as a function of normalized L_1 and L_2. The optimal L_1 value, i.e. $L_{1\mathrm{opt}}$, occurs at point A. In order to illustrate how the plots are interpreted, the trajectory of an arbitrary starting point Ψ is plotted. According to the signs of the arrows, L_1 will increase and L_2 will decrease until point A is reached. It is interesting to observe the case where L_2 is equal to $L_{1\mathrm{opt}}$. In this case, L_1 will converge to point B if there is a small negative deviation. In this situation, L_1 and L_2 switch their values, i.e. $L_1 = L_{2\mathrm{opt}}$ and $L_2 = L_{1\mathrm{opt}}$. A similar behavior for L_2 can be seen in figure 6(b). Such behavior is undesirable, because the damping resistors R_i are set only for a specific mode (see table 2). However, this behavior is easily avoided by enforcing restrictions on the range of L_1 and L_2.

4. Experiments

In this section, relative phase adaptation is used to tune and maintain the optimal performance of a two and four mode resonant shunt damping circuit. The experiments were carried out on a cantilevered piezoelectric laminate beam at the Laboratory for Dynamics and Control of Smart Structures, University of Newcastle, Australia.

4.1. Synthetic impedance

As shown in figure 2, an arbitrary impedance can be implemented with a voltage measurement, signal filter, and current source. A dSpace 1005 system was used to implement all of the filtering and processing tasks. More details on the construction of the analog electronics can be found in [7].

4.2. Piezoelectric laminated cantilever beam structure

The experimental structure is a uniform aluminum beam with rectangular cross-section. The dimensions and physical properties are displayed in figure 7 and table 1. Two identical piezoelectric patches are laminated symmetrically onto the front and back faces of the beam. One patch generates strain disturbance in the beam. The adaptive shunt impedance is connected to the other patch. The mechanical and piezoelectric properties of the two patches are summarized in table 1. Since the currents are defined in the digital implementation of the synthetic transfer-function $Y(s)$, they are already available for the relative phase adaptation and do not have to be measured.

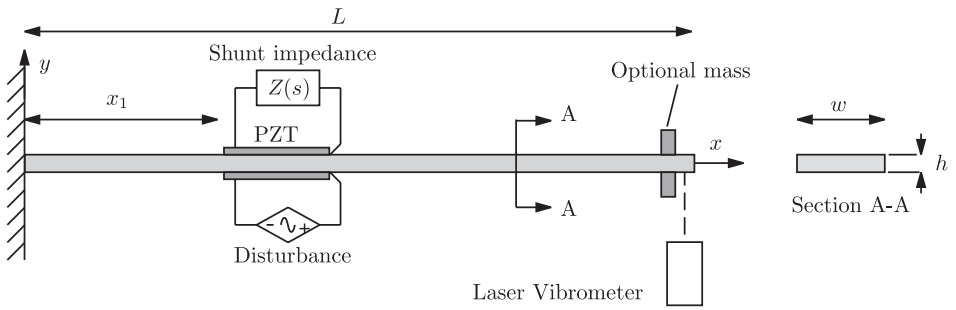

Figure 7. Experimental piezoelectric laminated cantilever structure.

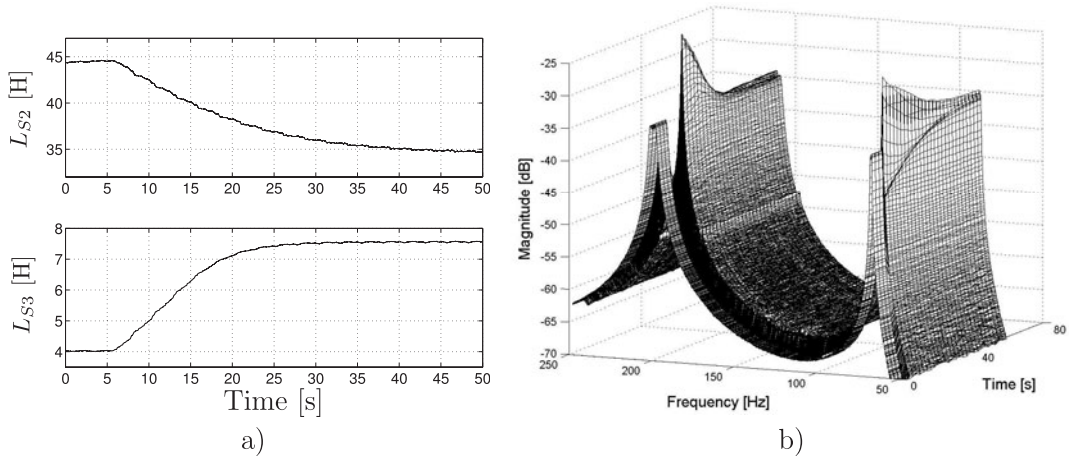

Figure 8. (a) Time evolution of the inductance values L_{S2} and L_{S3} after a step change in the resonance frequencies. (b) Magnitude of $G_v(s)$ as a function of time, after a change in the resonance frequencies.

Table 1. Properties of the cantilever beam, the piezoelectric patch and the additional weight.

Name	Symbol	Value
Cantilever beam		
Length	L	450 mm
Width	W	50 mm
Thickness	h	3 mm
Young's modulus	E	65×10^9 N m^{-2}
Density	ρ	10.6 kg m^{-2}
Piezoelectric patch		
Disturbance location	x_1	130 mm
Shunt location	x_1	130 mm
Length	L_p	75 mm
Width	W_p	25 mm
Thickness	h_p	2.5 mm
Capacitance	C_p	104 nF
Young's modulus	E_p	62×10^9 N m^{-2}
Strain constant	d_{31}	-320×10^{-12} m V^{-1}
Electromechanical coupling factor	k_{31}	0.44
Stress constant/ voltage coefficient	g_{31}	-9.5×10^{-3} m N^{-1}

4.3. Two mode damping

In a first study, the second and third mode of the cantilever beam are damped using the adaptive multi-mode resonant shunt. The shunt circuit component values are summarized in table 2 (f_2 and f_3). The tuning values α_i are set such that the deviation of L_i around the optimal value is not too high. These deviations appear because the spectrum of the excitation is normally slightly varying in time.

4.3.1. Modal frequency variations. In this experiment, the behavior of the adaptive shunt is examined subject to a step change in the structural resonance frequencies. The modal frequencies are disturbed by attaching an additional mass to the cantilever beam. The second mode moves from 69.5 to 71.2 Hz, and the third mode from 201.2 to 192.6 Hz. In figure 9(1), the multi-mode shunt is optimally tuned and the corresponding inductances are $L_{S2} = 44.5$ H and $L_{S3} = 4$ H (see figure 8(a)). The additional mass is then attached, effectively detuning the multi-mode shunt. In plots 3–6 of figure 9, the relative phase adaptation is retuning until the optimum is reached again in plot 6. The tuning behavior can also be observed in figure 8(a) where the initial inductances are $L_{S2} = 44.5$ H and $L_{S3} = 4$ H (optimal). After the additional mass is attached, the inductance values tune to $L_{S2} = 34.5$ H and $L_{S3} = 7.5$ H. The evolution of the magnitude transfer-function $G_v(r, s)$ during adaptation is shown in figure 8(b).

4.3.2. Piezoelectric capacitor changes. In this experiment, the effect of a change in piezoelectric capacitance C_p is investigated. In figure 10(1), the multi-mode shunt is optimally tuned, but the damping of the branches is slightly decreased in order to show better the tuning. In plot 2, C_p is artificially

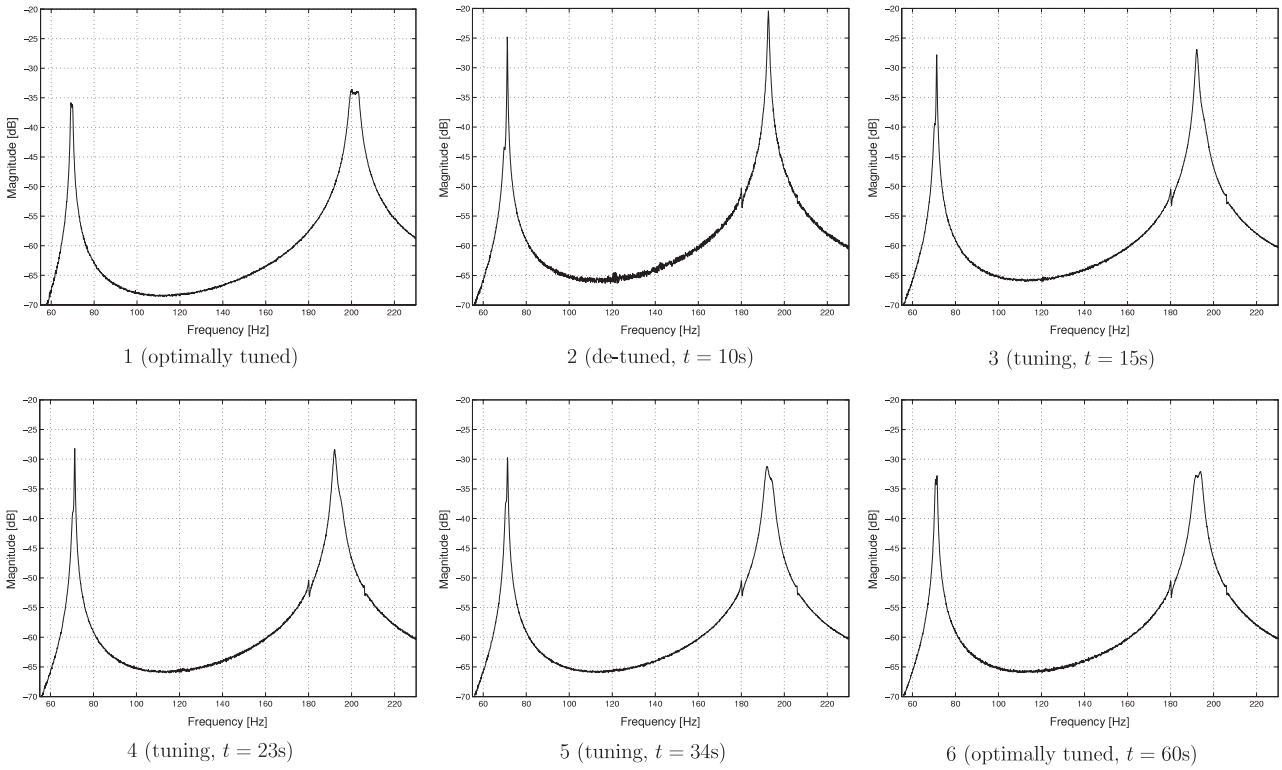

Figure 9. Magnitude of the transfer functions $G_v(r, s)$ during adaptation. At time $t = 10$ s, the modal frequency changes. In plots 3–6, the relative phase adaptation is retuning until the optimum is reached again in plot 6.

Table 2. Properties of the multi-mode shunt circuit.

$f_1 = 11.62$ Hz		$f_2 = 69.5$ Hz		$f_3 = 201.2$ Hz		$f_4 = 401.5$ Hz	
Property	Value	Property	Value	Property	Value	Property	Value
L_{S1} (kH)	$[5 \leftrightarrow 8]$	L_{S2} (H)	$[25 \leftrightarrow 45]$	L_{S3} (H)	$[7 \leftrightarrow 8]$	L_{S4} (H)	$[0.8 \leftrightarrow 2]$
R_{S1} (Ω)	2000	R_{S2} (Ω)	1350	R_{S3} (Ω)	900	R_{S4} (Ω)	210
L_{F1} (H)	9576	L_{F2} (H)	237.6	L_{F3} (H)	29.69	L_{F4} (H)	7.696
C_{F1} (nF)	20	C_{F2} (nF)	20	C_{F3} (nF)	20	C_{F4} (nF)	20
α_1	1000	α_2	1.5	α_3	1	α_4	0.5

decreased. As a result, in plots 3–5, one can observe an adaptation of L_{S2} and L_{S3} that counteracts the capacitance decrease. In plot 6, C_p is increased. The shunt is retuned in plots 7–9.

4.3.3. Sensitivity analysis. In this section, the sensitivity of the adaptation law is analyzed as in section 3.3. Figure 11(a) shows the tuning direction of L_{S2}, i.e. $\operatorname{sgn}\left(g_{\mathrm{LP}}^2(t) * [I_2(t)v(t)]\right)$, as a function of L_{S2} and L_{S3}. As desired, the tuning direction is dependent only on L_{S2}. The tuning direction of L_{S3} is shown in figure 11(b) and it is dependent only on L_{S3}. From these plots we can ascertain that there is no cross correlation between the tuning of L_{S2} and L_{S3}, and that each current-flowing branch operates independently over the range examined.

4.4. Four mode damping

For the purpose of demonstration, the experiments in the previous section were performed for two modes only. It is straightforward to apply the technique to damp a higher number of modes. This section briefly demonstrates the adaptive shunt damping of four structural modes. The frequency response of an optimally tuned four mode shunt circuit is shown in figure 12(a). In figure 12(b) the behavior of each inductance value is shown subject to step changes in the structural resonance frequencies. The disturbance in the structural resonance frequencies is achieved by changing the position of an additional point mass. At time 60 s the position of the mass is changed, then changed to another position at time 300 s. One can see that the branches of the shunt are retuned within about one minute and then remain at the optimal value.

5. Conclusion

Standard multi-mode resonant shunts are known to be highly sensitive to variations in the transducer capacitance and structural resonance frequencies. In many practical applications, such shunt circuits require online component value optimization.

Former adaptive techniques based on RMS minimization require excessively long convergence times and are prone

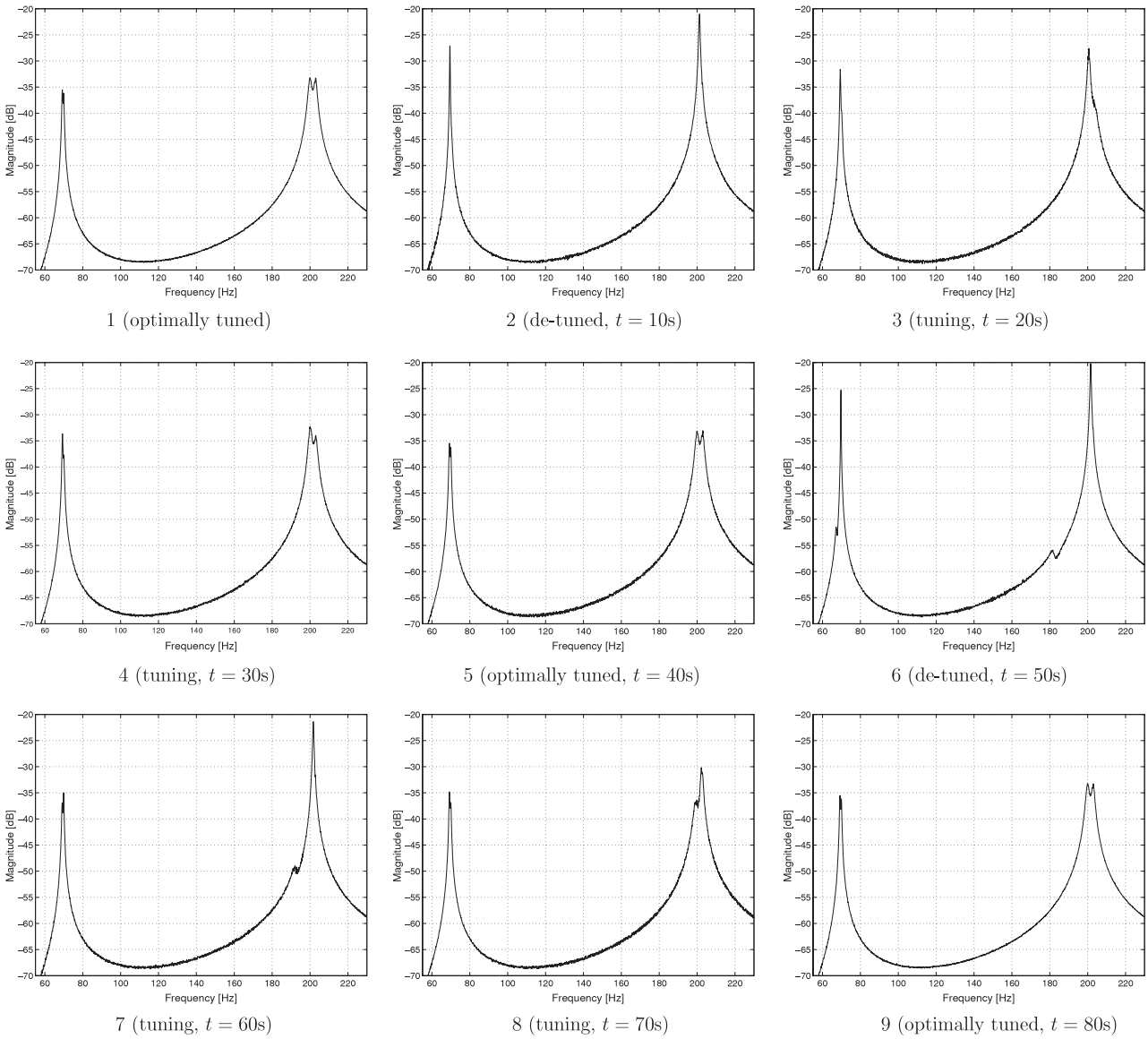

Figure 10. Transfer functions $G_\nu(r, s)$ during adaptation to a change in the piezoelectric capacitance. In plot 2, C_p is artificially decreased. As a result, in plots 3–5, one can observe an adaptation of L_{S2} and L_{S3} that counteracts the capacitance decrease. In plot 6, C_p is increased and the shunt is retuned in plots 7–9.

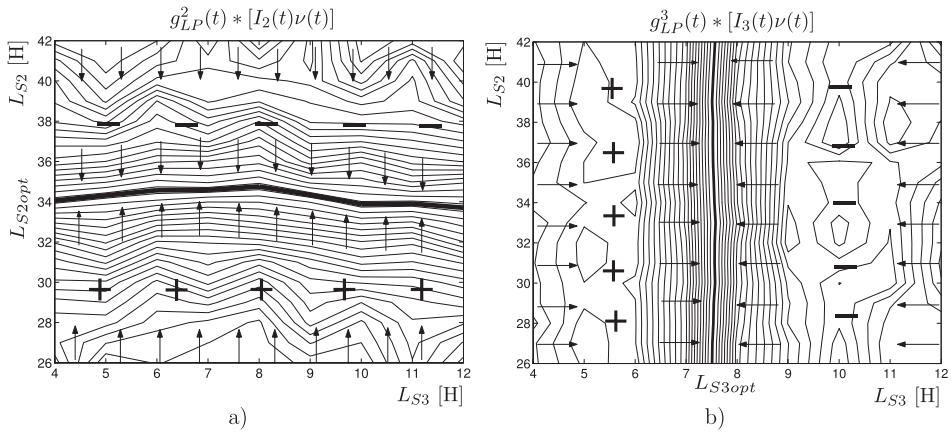

Figure 11. Measured tuning direction (a) $dL_{S2}(L_{S2}, L_{S3})$ and (b) $dL_{S3}(L_{S2}, L_{S3})$ of L_{S2} and L_{S3}, i.e. $\mathrm{sgn}\left(g^2_{\mathrm{LP}}(t) * [I_2(t)\nu(t)]\right)$ and $\mathrm{sgn}\left(g^3_{\mathrm{LP}}(t) * [I_3(t)\nu(t)]\right)$.

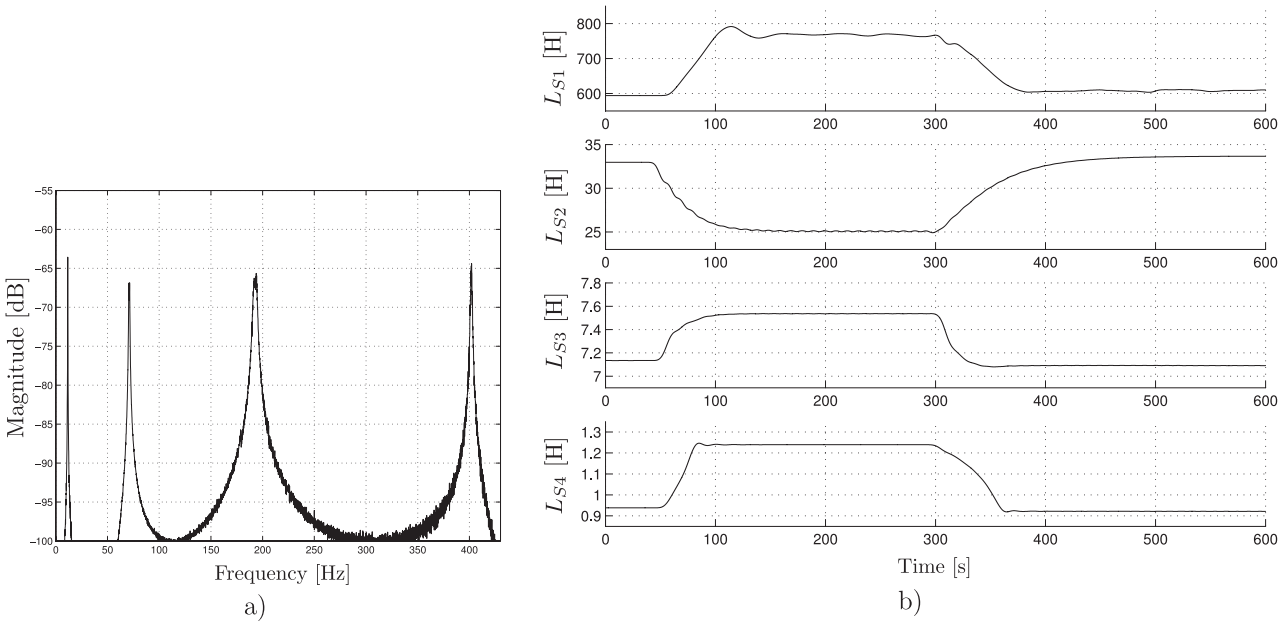

Figure 12. (a) The transfer function $G_v(r, s)$ with an optimally tuned four mode shunt circuit. (b) Inductance values of the multi-mode shunt subject to step changes in the structural resonance frequencies. At time 60 s the position of the mass is changed, then changed to another position at time 300 s.

to misadjustment. In this paper, a new technique has been introduced for the online adaptation of resonant piezoelectric shunt damping circuits. The adaptation law is based on minimizing the relative phase difference between a vibration reference signal and the shunt branch current.

Experiments have demonstrated the adaptive shunt damping of up to four structural modes simultaneously. Optimal performance was maintained in the presence of artificial variations in structural resonance frequency and transducer capacitance. The technique is easy to implement, requires little additional computation or electronics, and is suitable for practical applications.

Acknowledgments

Support for this research has been provided by grants from ETH (Zurich), EMPA (Dubendorf) and ARC (Australia). The experimental facilities were provided by the Laboratory for Dynamics and Control of Smart Structures (LDCSS).

References

[1] Behrens S, Fleming A J and Moheimani S O R 2003 A broadband controller for shunt piezoelectric damping of structural vibration *Smart Mater. Struct.* **12** 18–28

[2] Behrens S, Moheimani S O R and Fleming A J 2003 Multiple mode current flowing passive piezoelectric shunt controller *J. Sound Vib.* **266** 929–42

[3] Corr L R and Clark W W 2002 Comparison of low-frequency piezoelectric switching shunt techniques for structural damping *Smart Mater. Struct.* **11** 370–6

[4] Corr L R and Clark W W 2003 A novel semi-active multi-modal vibration control law for a piezoceramic actuator *J. Vib. Acoust. Trans. ASME* **125** 214–22

[5] Fleming A J, Behrens S and Moheimani S O R 2002 Optimization and implementation of multi-mode piezoelectric shunt damping systems *IEEE/ASME Trans. Mechatronics* **7** 87–94

[6] Fleming A J and Moheimani S O R 2003 Adaptive piezoelectric shunt damping *Smart Mater. Struct.* **12** 36–48

[7] Fleming A J and Moheimani S O R 2003 Improved current and charge amplifiers for driving piezoelectric loads *Smart Structure and Materials—Damping and Isolation; Proc. SPIE* **5052** 242–52

[8] Fuller C R, Elliott S J and Nelson P A 1996 *Active Control of Vibration* (New York: Academic)

[9] Hagood N W and Von Flotow A 1991 Damping of structural vibrations with piezoelectric materials and passive electrical networks *J. Sound Vib.* **146** 243–68

[10] Hanselka H 2002 Adaptronik und Fragen zur Systemzuverlässigkeit *ATP, Automatisierungstechnische Praxis* **2** 44–9

[11] Hollkamp J J 1994 Multimodal passive vibration suppression with piezoelectric materials and resonant shunts *J. Intell. Mater. Syst. Struct.* **5** 49–56

[12] Hollkamp J J and Starchville T F Jr 1994 A self-tuning piezoelectric vibration absorber *J. Intell. Mater. Syst. Struct.* **5** 559–65

[13] Ljung L 1999 *System Identification: Theory for the User* (Englewood Cliffs, NJ: Prentice-Hall)

[14] Meirovitch L 1996 *Elements of Vibration Analysis* 2nd edn (Sydney: McGraw-Hill)

[15] Moheimani S O R, Fleming A J and Behrens S 2003 On the feedback structure of wideband piezoelectric shunt damping systems *Smart Mater. Struct.* **12** 49–56

[16] Niederberger D, Behrens S, Fleming A J, Moheimani S O R and Morari M 2003 Adaptive electromagnetic system for shunt damping *IEEE/ASME Trans. Mechatronics* submitted

[17] Niederberger D, Morari M and Pietrzko S 2003 Adaptive resonant shunted piezoelectric devices for vibration suppression *Smart Structures and Materials—Smart Structures and Integrated Systems; Proc. SPIE* **5056** 213–24

[18] Richard C, Guyomar D, Audigier D and Bassaler H 2000 Enhanced semi-passive damping using continuous switching of a piezoelectric devices on an inductor *Smart Structures and Materials—Damping and Isolation; Proc. SPIE* **3989** 288–99

[19] Riodan R H S 1967 Simulated inductors using differential amplifiers *Electron. Lett.* **3** 50–1
[20] Wu S Y 1996 Piezoelectric shunts with parallel R–L circuit for structural damping and vibration control *Smart Structures and Materials—Passive Damping and Isolation; Proc. SPIE* **2720** 259–69
[21] Wu S Y 1999 Multiple PZT transducers implemented with multiple-mode piezoelectric shunting for passive vibration damping *Smart Structures and Materials—Passive Damping and Isolation; Proc. SPIE* **3672** 112–22
[22] Wu S Y 2000 Broadband piezoelectric shunts for structural vibration control *Patent Specification* No. 6,075,309
[23] Wu S Y and Bicos A S 1997 Structural vibration damping experiments using improved piezoelectric shunts *Smart Structures and Materials—Passive Damping and Isolation; Proc. SPIE* **3045** 40–50